Experimental Evidence of Interpenetration and High Ion Temperature in Colliding Plasmas

O. Rancu, P. Renaudin, C. Chenais-Popovics, H. Kawagashi,* and J. C. Gauthier
Laboratoire pour l'Utilisation des Lasers Intenses, Ecole Polytechnique, 91128 Palaiseau, France

M. Dirksmöller, T. Missalla, I. Uschmann, and E. Förster
Max-Planck-Arbeitsgruppe "Röntgenoptik", Friedrich-Schiller Universität, Max-Wien-Platz 1, D07743 Jena, Germany

O. Larroche and O. Peyrusse
Centre d'Etudes de Limeil-Valenton, 94195 Villeneuve-Saint-Georges Cedex, France

O. Renner and E. Krouský
Institute of Physics, Academy of Sciences of the Czech Republic, Prague, Czech Republic

H. Pépin
INRS Energie-Matériaux, Université du Québec, C.P. 1020, J3X1S2, Varennes, Québec, Canada

T. Shepard
Lawrence Livermore National Laboratory, Livermore, California 94550
(Received 28 April 1995)

The collision of two plasmas produced from laser-exploded Al/Al and Al/Mg foils has been studied by x-ray diagnostics over a wide range of experimental conditions. Ion temperatures of about 10 keV have been unambiguously inferred from Doppler broadening. The interpenetration distances have been determined by the spatial extent of Mg and Al ion emission. The comparison of experimental data with multifluid and atomic physics simulations gives a good understanding of the localization and dynamics of the kinetic to thermal energy transfer in the interpenetration regime.

PACS numbers: 52.50.Jm, 52.25.Dg, 52.65.–y, 52.70.–m

The study of the collision of two counterstreaming laser-produced plasmas has been motivated essentially by inertial confinement fusion with indirect drive [1] and by the need to create a long scale-length homogeneous plasma for laser interaction and x-ray laser studies [2,3]. Two main experimental schemes have been explored: the collision of blowoff plasmas produced at the front of thick laser-irradiated targets [4–11] and the collision of the plasmas produced at rear sides of two laser-exploded thin foils [12].

The present work is focused on the collision of Al/Al and Al/Mg laser-exploded foils. In this configuration, a wide range of plasma parameters is explored by changing the intertarget distance and laser irradiance giving access to the very interesting regime where the ion-ion mean free path is comparable to the plasma characteristic dimensions. In this regime, interpenetration occurs and gives rise to "soft" stagnation [6]. The localization and dynamics of the transfer of ion kinetic energy into electron and ion thermal energy is at present poorly understood experimentally. In our work, comparison of x-ray images and spectra with multifluid simulations have actually evidenced high ion temperatures (in the 10 keV range) and interpenetration of the two different ionic species.

Two frequency-doubled beams of the Nd glass laser of the LULI facility ($\lambda = 0.53$ μm, $\Delta t = 600$ ps) were focused perpendicular to the targets through 250-mm-focal-length lenses and random-phase plates to obtain homogeneous 200-μm-diameter FWHM focal spots. The laser irradiance was varied between 3×10^{13} and 6×10^{13} W/cm^2. The targets were either two aluminum thin foils (0.8 μm thick) or an aluminum foil in front of a magnesium foil (1.0 μm thick). The intertarget distance was varied from 450 to 900 μm. The diagnostics probed the x-ray emission perpendicular to the laser axis. Two toroidally bent quartz crystals imaged the $1s^2$-$1s3p$ (He-β, $\lambda = 6.635$ Å) emission of aluminum with a spatial resolution of 35 μm onto two cathodes of a 120-ps-resolution framing camera gated at different times [13]. This line was chosen because He-like ions emit in a wide range of electron temperatures. A $n = 1 \rightarrow 3$ line offers a good compromise to minimize both Stark broadening and reabsorption. Two time-integrating spectrometers viewed the intertarget space. One was a flat ADP crystal with a slit of 35 μm recording the 5.5–7 Å region, i.e., the He-like and H-like lines of aluminum and H-like lines of magnesium. The other one was a vertical dispersion variant of the Johann (JV) spectrometer [14]. A quartz (10.0) crystal bent to a radius of 76.8 mm was set to record the spectrum in a narrow region including the aluminum He-β line. The spectrometer provided high spectral resolution (4000–1400 for 200–700 μm plasma size) to measure the ion temperature from Doppler broadening. The spatial resolution in the

 0031-9007/95/75(21)/3854(4)$06.00

direction perpendicular to the dispersion plane was limited to 20 μm by the pixel size of the charge coupled device detector. The high sensitivity of this instrument was found very useful to measure the interpenetration distance, defined as the total distance over which either the aluminum He-β or the magnesium Ly-δ lines were visible above the detector threshold in the opposite half target space.

The data obtained on the two spectrometers have been simultaneously analyzed to measure unambiguously the electron and ion temperatures. A spectrum was simulated with the collisional-radiative code FLY, the time-dependent version of RATION [15], with a time variation deduced from the time-resolved monochromatic images, which showed that the He β line was emitted only during 150 ps FWHM. Figure 1 gives the results in the case of an intertarget distance d_i of 560 μm and a laser irradiance I_l of 6×10^{13} W/cm^2. The high-resolution spectral profile of the He-β line measured with the JV spectrometer was fitted by varying the ion temperature and the radial size of the plasma [see Fig. 1(a)]. The He-like and H-like spectrum measured on the flat-crystal spectrometer was fitted using the same plasma size, and by varying the electron temperature and density [see Fig. 1(b)]. Reabsorption effects and instrumental and Stark broadening were taken into account in the analysis. We note that the Stark width

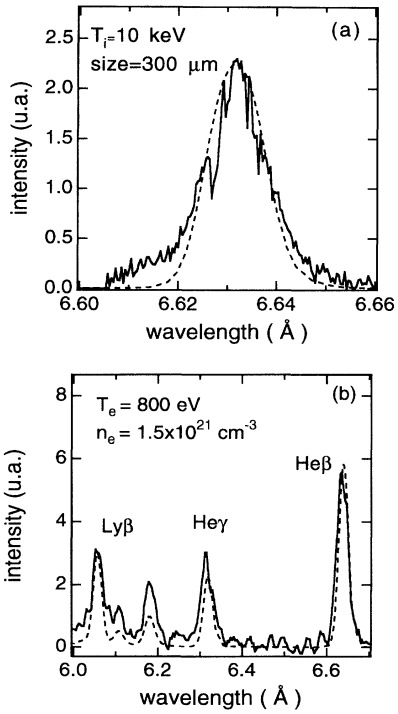

FIG. 1. Spectra obtained at 6×10^{13} W/cm^2 laser irradiance and 560 μm target separation (solid lines), compared with the best fit calculated with the code FLY (dashed lines). (a) JV spectrometer; (b) flat crystal spectrometer.

of the He-β line was less than 2 mÅ for electron densities found in the collision region.

Radial gradients and Doppler shifts due to lateral expansion were neglected. Indeed, the comparison of the focal spot diameter with the time-resolved radial size of the He-β line emission region during the collision suggests that lateral flow velocities are small. These assumptions were further checked using LASNEX 2D simulations. These predicted that the lateral velocity in the high-electron-temperature region was around 2×10^6 cm/s, inducing Doppler shifts of order 0.5 mÅ, i.e., much smaller than the 10 mÅ Doppler width expected for an ion temperature of 10 keV. The results of these simulations should be regarded as upper limits since single fluid 2D hydrodynamic codes are expected to overestimate the lateral expansion and velocity.

The electron and ion temperatures measured with the procedure described previously are shown in the third and fourth columns of Table I for different experimental conditions. They are determined at the center of the intertarget space, and averaged over the 35μm spatial resolution of the flat crystal spectrometer. The measured electron density is of order $(1-2) \times 10^{21}$ cm^{-3} for the range of parameters covered in Table I. The size of the plasma is 250 $\pm$ 50 μm for 450 μm intertarget distance and 650 $\pm$ 50 μm for 900 μm intertarget distance. Table I shows that T_i remains of the same order of magnitude as T_e for the lower laser irradiance case, increasing slightly as a function of target separation. When the laser irradiance is increased, the ion temperature reaches 10 keV in the two cases of 450 and 600 μm intertarget distance and the electron temperature stays around 800 eV.

Evidence of plasma interpenetration was obtained primarily with the JV spectrometer. The spatial extent of the Al He-β and Mg Ly-δ lines emitted from both foils was measured along the intertarget axis. We note that this spectroscopic method shows the interpenetration in the regions that are heated at the appropriate temperature to emit the observed x-ray lines. For a low irradiance of 3×10^{13} W/cm^2, monochromatic imaging of the He-β Al line showed no interpenetration. Figure 2 shows the interpenetration distance measured as a function of target separation for a laser irradiance of 6×10^{13} W/cm^2. This distance increases with the target separation. An abrupt change of plasma conditions occurs for a laser irradiance between 3×10^{13} and 6×10^{13} W/cm^2. Indeed, we note experimental evidence of interpenetration and increasing ion temperatures only for high enough laser irradiances.

Numerical simulations have been performed with the multifluid code MULTIF to understand better the interpenetration and the exchange of ion kinetic energy to thermal energy. MULTIF is a multispecies, Eulerian, 1.5D fluid code in which the lateral expansion is taken into account through a self-similar model [16]. The code uses the improved flux-corrected transport modules of Boris [17], and flux-limited Spitzer conductivity. The early laser

TABLE I. Plasma parameters determined at target midplane for different intertarget distances and laser intensities.

I_l (W/cm^2)	d_i (μm)	T_e (keV)	T_i (keV)	$T_{e,\max}$ (keV)	$T_{i,\max}$ (keV)	$T_{i,D}$ (keV)
3×10^{13}	450	0.35 ± 0.1[a]	0.35 ± 0.2[a]	0.35[b]	0.40[b]	
3×10^{13}	600	0.75 ± 0.2[a]	1.00 ± 0.3[a]	0.50[b]	6[b]	<2.5 [b]
3×10^{13}	900	0.80 ± 0.3[a]	0.80 ± 0.3[a]	0.55[b]	4[b]	<1.3 [b]
6×10^{13}	450	0.80 ± 0.2[a]	10 ± 3[a]	0.98[b]	27[b]	5.9[b]
6×10^{13}	600	0.80 ± 0.2[a]	10 ± 3[a]	1.00[b]	20[b]	7.1[b]
6×10^{13}	900	0.90 ± 0.3[a]	3 ± 1[a]	0.85[b]	18.5[b]	5.3[b]

[a]Experiment.
[b]Simulation.

absorption and foil acceleration stages are modeled by the 1.5D fluid code FILM [18]. A simple estimate of radiative cooling and ionization is made with a multispecies local thermodynamic equilibrium calculation of ionization states. The output of this code was postprocessed by the detailed spectroscopy model TRANSPEC [19] to compare the calculated x-ray emission of the plasma directly with the experimental results. Figure 2 shows the excellent agreement between the interpenetration distance determined from the calculated Al He-β axial emission profile and experiment. In this comparison, lateral plasma reabsorption effects and instrument resolution are taken into account.

Multifluid simulations were run for experimental irradiances and intertarget distances. The maximum values of the plasma parameters $T_{e,\max}$ and $T_{i,\max}$ at target midplane (see Table I) and their time variation (see Fig. 3) demonstrate the very different regimes covered by our range of experimental conditions. For a low irradiance of 3×10^{13} W/cm^2, the electron density is very high, around 10^{22} cm^{-3}, and the electron temperature is slightly higher than the temperature calculated in a freely expanding plasma. The ion temperature does not increase much, with a maximum around 6 keV; this increase is sharply peaked in time and space (FWHM around 50 ps and 20 μm). This explains why the time-integrated measurements give similar results for T_i and T_e. For a laser irradiance of 6×10^{13} W/cm^2, the temperatures calculated for 450 and 600 μm are very similar, as in the experiment. The electron density is of order 10^{21} cm^{-3}, and the ion temperature rises to 20–27 keV (see Fig. 3). When the distance is increased to 900 μm, all the maxima decrease, and the most striking feature is that the maximum of T_i occurs much later at target midplane than the maxima of n_e and T_e. The stagnation time coincides with the ion temperature peak. The spatial extent of the parameters along the intertarget axis was also increases with d_i. This confirms

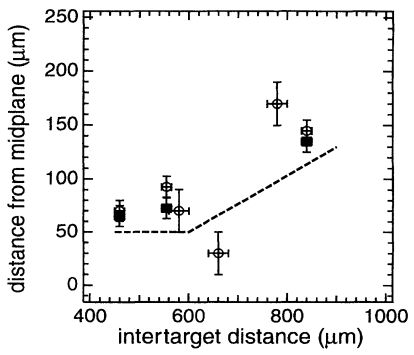

FIG. 2. Interpenetration distance measured from midplane as a function of target separation for a laser irradiance of 6×10^{13} W/cm^2 with the He-β Al line (circles), and Ly-δ Mg line (squares). The dashed line gives the MULTIF + TRANSPEC predictions for He-β.

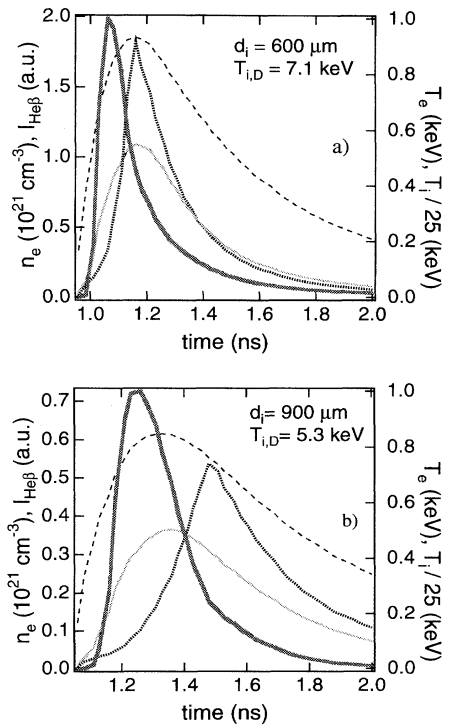

FIG. 3. Temporal evolution of the plasma parameters as calculated by MULTIF and of the maximum of the He-β line emission given by MULTIF + FLY, at target midplane, for a laser irradiance of 6×10^{13} W/cm^2. Intertarget distance of 600 μm (a), and 900 μm (b). Solid line: n_e; dashed line: T_e; dotted line: T_i; thick solid line: He-β emission.

that at wide target separations, interpenetration begins to play an important role in the collision.

Figure 3 also shows the time variation of the maximum of the He-β line profile calculated with MULTIF + FLY. These results clearly explain the difference between the peak calculated and measured ion temperatures. First, the plasma parameters are varying so rapidly that the ionization distribution departs from equilibrium. In particular, the predicted He-β line emission does not follow the variation of the electron density and temperature closely, but instead lasts for only 100 to 200 ps, in agreement with the time-resolved monochromatic imaging measurements. Due to this short duration, the He-β emission samples the ion temperature over a comparable time scale. Second, Doppler broadening measurements give an ion temperature very different from the theoretically expected maximum of T_i. This effect is particularly important in the wide separation regime when the maximum of T_i occurs long after the peak of electron density and temperature. The spectral width of the time-integrated He-β line profile at the center of the intertarget space provides a value of the ion temperature, $T_{i,D}$, which is reported in Table I. $T_{i,D}$ is very consistent with the experimental data for the high-laser-intensity case and shows the same decrease at high intertarget separation. This decrease is experimental evidence that the plasmas interpenetrate.

The various regimes observed in the simulation and the experiment can be interpreted via the collisionality parameter $\zeta = D/C_s\tau_{ii}$, where D is a characteristic dimension of the plasma collision geometry, C_s the ion sound speed, and τ_{ii} the ion-ion collision time [6]. In the present case of thin foils, the relevant distance D is the foil thickness, making the density $\times$ distance product independent of time. This is justified as far as lateral expansion can be neglected, which is approximately valid up to collision time, as seen in our 1.5D simulations. Hence, the only remaining parameter governing collisionality is the foil velocity at collision time, which is expected to increase as the laser intensity and/or the initial foil separation increase. The ζ values found from our experimental data, taking velocity values from corresponding simulations, range from about 1 to 0.04 when one goes from the case of lowest intensity and shortest separation to the case of highest intensity and largest separation. Thus, the transition from collision to interpenetration is indeed expected to be observed.

In conclusion, we have investigated the interaction of two plasmas in a wide range of experimental parameters covering the full range of conditions from quasicollisionless to strongly collisional. For low laser irradiance (3×10^{13} W/cm^2), the counterstreaming plasma densities are high and their velocities are small. The plasmas do not interpenetrate, and the ion kinetic energy is transferred only in a small region at the center of the intertarget space and moderately heats the ions and electrons. At higher laser irradiance (6×10^{13} W/cm^2), the relative velocity of the two plasmas is higher. For $d_i = 450$–600 μm, the energy transfer occurs early, interpenetration remaining moderate in a regime of high density and low velocity of the counterstreaming plasmas. For larger target separation (900 μm), the density decreases and the velocity increases. The electron and ion temperature profiles are spread over a much larger intertarget distance, and the energy transfer occurs in a wide region around the target midplane. Stagnation, i.e., maximum T_i and zero relative velocity, occurs much later than the maximum of n_e, T_e, and He-β line emission. The decrease of T_i and increase of the interprenetration distance at large target separation indicate that the interpenetration mechanism is not inhibited by other processes such as instabilities and turbulence.

The authors thank the LULI staff, in particular, C. Montheil and R. Koenig for their help during the experiments, and the very skillful target preparation of the Institute of Nuclear Physics at Paris-Sud University. This work was supported by the Centre National de la Recherche Scientifique, by the EU HCM Contract No. ERBCHRXCT930377, and by the Grant Agencies of the Czech Republic.

*Present address: PNC, Muramatsu, Tokyo, Japan.

[1] R.L. Kauffman *et al.*, Phys. Rev. Lett. **73**, 2320 (1994).
[2] B. Yaakobi *et al.*, IEEE Trans. Plasma Sci. **16**, 505 (1988).
[3] C. Stöckl and G.D. Tsakiris, Laser Part. Beams **9**, 725 (1991).
[4] R.A. Bosch *et al.*, Phys. Fluids B **4**, 979 (1992).
[5] R.L. Berger *et al.*, Phys. Fluids B **3**, 3 (1991).
[6] P.W. Rambo and J. Denavit, Phys. Plasmas **1**, 4050 (1994).
[7] C.A. Back, R.L. Kauffman, P.M. Bell, and J.D. Kilkenny, Rev. Sci. Instrum. **66**, 764 (1995).
[8] D. Jurazcek (private communication).
[9] A. Decoster, M. Demoulins, and G. Schurtz (private communication).
[10] O. Larroche, Phys. Fluids B **5**, 2816 (1993).
[11] M. Wilke *et al.*, SPIE Proceedings Vol. 2523 [SPIE–International Society for Optical Engineering, Bellingham, WA (to be published)].
[12] R.J. Taylor, A.J. MacKillon, R. Mansukhani, and O. Willi, in DRAL Annual Report, 1994 (unpublished), p. 69.
[13] M. Dirksmöller *et al.*, Opt. Commun. (to be published).
[14] O. Renner *et al.*, Laser Part. Beams **12**, 539 (1994).
[15] R.W. Lee, B.L. Whitten, and R.E. Strout, J. Quant. Spectrosc. Radiat. Transfer **32**, 91 (1984).
[16] J. Virmont, N. Grandjouan, and A. Klisnick, LULI Report 1990, available upon request to the authors.
[17] D.L. Book, J.P. Boris, and S.T. Zalesak, *Finite Difference Techniques for Vectorized Fluid Dynamics Calculations,* edited by D.L. Book (Springer-Verlag, New York, 1981), p. 29.
[18] J.C. Gauthier *et al.*, J. Phys. D **16**, 321 (1983), and references therein.
[19] O. Peyrusse, Phys. Fluids B **4**, 2007 (1992).